RESEARCH ARTICLE
SPACE PHYSICS: MAGNETOSPHERIC PHYSICS

Earth and Planetary Physics
8: 382–390, 2024
doi: 10.26464/epp2024018

Effect of interplanetary magnetic field B_x on the polar electrojets as observed by CHAMP and Swarm satellites

Hui Wang*, ChengZhi Wang, and YunFang Zhong

Department of Space Physics, School of Electronic Information, Wuhan University, Wuhan 430072, China

Key Points:

- The influence of the IMF B_x sign on PEJ current density displays local time, seasonal, and hemispherical differences.
- The IMF B_x sign has stronger effect on PEJs around noon in the local summer hemisphere; around midnight in the local winter hemisphere.
- The positions of PEJs in the Northern and Southern hemispheres are unconjugated with respect to the sign of IMF B_x.

Citation: Wang, H., Wang, C. Z., and Zhong, Y. F. (2024). Effect of interplanetary magnetic field B_x on the polar electrojets as observed by CHAMP and Swarm satellites. *Earth Planet. Phys.*, *8*(2), 382–390. http://doi.org/10.26464/epp2024018

Abstract: Based on 16 years of magnetic field observations from CHAMP and Swarm satellites, this study investigates the influence of the Interplanetary Magnetic Field (IMF) B_x component on the location and peak current density of the polar electrojets (PEJs). We find that the IMF B_x displays obvious local time, seasonal, and hemispherical effects on the PEJs, as follows: (1) Compared to other local times, its influence is weakest at dawn and dusk. (2) In the midnight sectors of both hemispheres, the IMF B_x tends to amplify the westward PEJ when it is <0 in the Northern Hemisphere and when it is >0 in the Southern Hemisphere; this effect is relatively stronger in the local winter hemisphere. (3) At noontime, the IMF B_x intensifies the eastward current when it is <0 in the Northern Hemisphere; in the Southern Hemisphere when it is >0, it reduces the westward current; this effect is notably more prominent in the local summer hemisphere. (4) Moreover, the noontime eastward current shifts towards higher latitudes, while the midnight westward current migrates towards lower latitudes when IMF B_x is <0 in the Northern Hemisphere and when it is >0 in the Southern Hemisphere.

Keywords: polar electrojet; interplanetary magnetic field B_x; local time asymmetry; hemispheric difference

1. Introduction

The polar electrojets (PEJs) constitute important components of high-latitude current systems. PEJs stream within the ionospheric *E* region perpendicular to both the electric and magnetic fields. Observations from ground-based magnetometers, rockets, satellites, and comprehensive model simulations, demonstrate that PEJs exhibit variations in local time, seasons, and hemispheres in response to changes in the interplanetary magnetic field (IMF) (e.g. Gjerloev and Hoffman, 2014; Guo JP et al., 2014; Huang T et al., 2017; Laundal et al., 2018a, b; Zhong YF et al., 2022; Wang H and Lühr, 2023, 2024; Wang YB, 2023).

Among the three components of IMF, IMF B_z in the north–south direction stands out as the primary factor influencing the development and characteristics of the polar current system. While the direct influence of IMF B_z on PEJ might be less pronounced than field-aligned currents (FACs), it can indirectly affect the strength and behavior of a PEJ by modulating the polar electric field and ionospheric dynamics (e.g. Huang T et al., 2017). PEJs show stronger intensity under southward IMF B_z compared to northward IMF B_z (e.g. Wang H et al., 2008; Huang T et al., 2017).

IMF B_y in the dawn–dusk direction causes dawn–dusk and hemispheric asymmetry in PEJs. Around noontime in the polar region, prominent DPY (Dayside Polar cap Y) PEJs emerge with their flowing direction and intensity controlled by the orientation of the IMF B_y (e.g. Friis-Christensen and Wilhjelm, 1975). The merging electric field, $\boldsymbol{E}_{\rm m}$, considers the collective influence of IMF B_z and B_y on the solar wind electric fields that effectively drive the magnetosphere–ionosphere interactions. The intensity of prominent PEJs was found to be controlled by the merging electric field (e.g. Huang T et al., 2017). Note that $\boldsymbol{E}_{\rm m}$ considers the direction of IMF B_z, while remaining symmetric regarding the polarity of IMF B_y.

However, recent work has revealed local time and hemispheric asymmetry in the auroral current system in relation to the orientation of IMF B_y (Wang H and Lühr, 2023). Generally, they found that the opposite signs of dipole tilt angle (the angle between the Earth's dipole axis and the Sun–Earth connection) and IMF B_y tend to enhance the westward PEJ in the dawn and midnight sectors, supporting the finding of Reistad et al. (2020). At *dawn*, this clear IMF B_y effect is roughly equal in both winter and summer hemispheres; however, at *midnight*, the effect is relatively stronger in the local winter hemisphere. At *noon*, the influence of IMF B_y is basically consistent with the dependence of DPY current on IMF B_y polarity, and the impact is stronger in the local summer hemi-

Correspondence to: H. Wang, h.wang@whu.edu.cn
Received 07 DEC 2023; Accepted 24 JAN 2024.
First Published online 01 MAR 2024.

sphere. At *dusk*, the effect of IMF B_y on the eastward PEJ is significantly weaker than that observed in the other local time sectors. Furthermore, the positions of the PEJ in the Northern Hemisphere (NH) and Southern Hemisphere (SH) are not conjugate; instead, their positions are related to the orientation of IMF B_y. For the eastward and westward PEJs, the variation of hemispheric latitude displacement of PEJ with IMF B_y polarity is completely opposite.

Unlike IMF B_y and B_z, IMF B_x does not appear to influence PEJ intensity. However, variations in IMF B_x are known to correlate with auroral intensity; thus, it might be that IMF B_x contributes to changes in the PEJ *pattern*. Elphinstone et al. (1990) found that NH aurora at dawn and dusk was weaker for IMF $B_x > 0$ than $B_x < 0$ under northward IMF condition. Shue et al. (2002) reported that the NH nighttime auroral power was higher for IMF $B_x < 0$ than for IMF $B_x > 0$ under similar IMF B_y conditions when IMF is southward. This specific IMF B_x effect was significant in both summer and winter. For northward IMF, such IMF B_x asymmetry was not observed due to weak aurora intensity. They concluded that hemispheric auroral power reached its highest level when all the components of IMF were negative. Reistad et al. (2014) found that the duskside aurora in the winter NH was brighter for IMF $B_x < 0$, while SH aurora was brighter for IMF $B_x > 0$. This distinctive impact of IMF B_x was clarified as due to asymmetric dayside reconnection — a northward shift of the dayside reconnection line for IMF $B_x > 0$ and a southward shift for IMF $B_x < 0$. As a consequence, the tail plasma sheet undergoes a reverse northward–southward directional shift (Cowley, 1981; Hoilijoki et al., 2014). Moreover, Kubyshkina et al. (2018) revealed that IMF B_x is important for the more frequent occurrence of substorms, based on Kivelson and Hughes (1990)'s theory regarding a lower threshold of substorm instability in a curved current sheet.

Through the analysis of a typical case of a magnetic storm event, Wang H et al. (2014) showed that, with a strong sunward IMF B_x, a new pair of strong field-aligned currents emerge at noon, with the poleward part flowing downward and the equatorward part flowing upward. By using multi-satellite and ground based observations, Laundal et al. (2018b) showed that the sign of IMF B_x changes FACs and ionospheric equivalent current by no more than 10% under southward IMF B_z conditions. Their work relied on average distribution maps of satellite-observed currents, sorted by IMF components. Additionally, their work extensively compared FACs to the findings of Reistad et al. (2014), but overlooked examination of PEJs in different local times and hemispheres. On the other hand, Kubyshkina et al. (2023) highlighted the obvious asymmetric polarity-dependent effects of IMF B_x, attributed to the dipole tilt effect on magnetotail stability and nightside reconnection. In winter, IMF $B_x > 0$ suppresses *AL* index while $B_x < 0$ increases *AL* under similar driving conditions. Their work focused primarily on exploring the influence of nighttime IMF B_x, neglecting investigation into its impact on the dayside. In summary, the local time and hemispheric differences in the impact of IMF B_x on PEJs have not been comprehensively investigated in the literature; further analysis is thus required to address these gaps.

This study is the first to provide a detailed investigation of IMF B_x effects on PEJ strength and latitude for different local times, seasons, and hemispheres, using observations from CHAMP and Swarm satellites. In the following section the data sets we studied and our methods are described. The statistical analysis of observations is presented in Section 3. A discussion and summary in the context of previous findings is presented in Sections 4 and 5.

2. Data: Sources and Processing Methods

The three European Space Agency Swarm satellites were launched on November 22, 2013, into a near-polar orbit with an inclination of 87.5°. The final orbit constellation was achieved on 17 April 2014. Swarm-A and Swarm-C fly side-by-side with a separation of 1.4° in longitude at about 450 km altitude; Swarm B flies at about 510 km with a slightly higher inclination. CHAMP was launched into a near-polar orbit on July 15, 2000 (87.3° inclination, 450 km altitude, orbital period of 93 min; Reigber et al., 2002) the mission lasted until September 2010.

PEJ strengths and positions were derived using scalar magnetic field data. Olsen (1996) first introduced the line current method for estimating the strength of an ionospheric PEJ. This method was later applied to CHAMP data, validated against ground-based observations (Ritter et al., 2004), and extended to Swarm data by Aakjær et al. (2016). The auroral electrojet is represented by a series of infinite line currents in the Earth's ionospheric *E* layer (about 115 km), each spaced 1° apart. The observed total field residuals undergo inversion via a least-squares fitting approach to derive the strength of each line current. This study is focused on estimating the zonal component of the PEJ, where positive values indicate eastward currents and negative values signify westward electrojet. To prevent false detections, peak absolute values need to fall within the range of 0.03 A/m to 3 A/m. In this analysis, a quasi-dipole (QD) coordinate system has been used (e.g., Richmond, 1995; Emmert et al., 2010).

This study utilizes CHAMP data from July 26, 2000 to September 4, 2010 and Swarm-A PEJ estimates from 17 April 2014 to 16 April 2020 (in total, more than 16 years of data). We select eastward PEJ peaks in the 15–20 MLT, and westward PEJ peaks in the 21–02 MLT and 03–08 MLT sectors from each auroral crossing. In the noontime, 09–14 MLT, both eastward and westward PEJ peaks are selected, because the direction of DPY current is related to the sign of IMF B_y. In this study we focus on the peak current density and location of the PEJs for several reasons. The PEJs represent a concentrated and intense current system within the auroral region. Typically, field-aligned currents flank PEJ peaks on both their poleward and equatorward sides. Thus, the PEJ peak location serves as a focal point representing the central region of auroral and field-aligned currents. The peak density of a PEJ frequently acts as an indicator of the magnitude of high latitude magnetic activity. Monitoring both peak density and location of a PEJ provides insights into geomagnetic activity and disturbances within the high latitude ionosphere.

The data are divided for two Lloyd seasons: June solstice (66 days before and after 1 July) and Dec. solstice (66 days before and after 1 January). As utilized in previous work (e.g. Huang T et al., 2015), the specific criterion used to select dominant IMF B_x events involves the IMF cone angle, calculated as the angle between the IMF vector and the Sun–Earth direction. It is calculated as

$$\arccos\frac{B_x}{\sqrt{B_x^2+B_y^2+B_z^2}}.$$

When the IMF cone angle is less than 30° or exceeds 150°, it signifies that IMF B_x component predominantly points toward the Sun or toward the Earth. Employing this angle criterion allows us to separate IMF B_x effect from other components of IMF, preventing potential contamination of results because of the Parker spiral configuration of the IMF.

The event numbers of auroral crossings for different IMF B_x cone angle are shown in Figure 1, categorized by local time, season, and hemisphere. This study focuses on periods with $E_m \leq 3$ mV/m since there are fewer events with IMF cone angle ≤30° and ≥150° during high E_m periods. Overall, the situation is more favorable for IMF B_x cone angle between 30° and 150°. Nevertheless, across each MLT bin, the number of events generally surpasses 50. However, despite our having an adequate number of samples in each local bin, the uneven distribution of events might impact the results. Notably, we have removed outliers from our analysis, which could help improve the stability of results. To further confirm the stability and generalizability of results, we conduct analyses on separate datasets, from either CHAMP (2000–2010) or Swarm (2014–2020) satellites. Our primary findings exhibit considerable consistency (figures not shown). These observations potentially indicate the reliability of the current statistical analyses. Future study may involve using additional observational data to validate the conclusions drawn in this work.

3. Statistical Results

PEJs typically exhibit an eastward (positive value) flow in the dusk sector, and a westward (negative value) flow in the dawn and midnight sectors; PEJ flow direction at noon can vary between eastward or westward, based on the IMF B_y polarity. Our primary focus in this study lies on assessing PEJ strength. Therefore, we use the absolute value of PEJ density in all local time sectors, treating both eastward and westward PEJ as positive values.

Figure 2 displays how absolute PEJ strength varies as a function of IMF B_x cone angle and magnetic local time. We calculate the mean absolute PEJ value within each local time, under all IMF B_x cone angle conditions, and then subtract these local time mean values from the recorded PEJ data in order to better represent PEJ variation as a function of IMF B_x cone angle, i.e., IMF B_x sign. The left panel of Figure 2 presents Northern Hemisphere results; the right panel, Southern Hemisphere results. Figures 2a–d are for positive PEJ around noon; Figures 2e–h are for negative PEJ around noon. When the IMF cone angle is greater than 90°, it represents IMF $B_x < 0$; when it is less than 90°, IMF $B_x > 0$. The closer the angle of IMF B_x is to 0° or 180°, the more influential the B_x component becomes. Conversely, when the angle is closer to 90°, the dominance shifts towards IMF B_y or B_z.

Obvious local time, seasonal, and hemispheric differences can be found when considering PEJ dependence on the cone angle. In local summer (Figures 2a, 2d, 2e, 2h), the dependence exhibits more significance on the dayside than on the nightside. Conversely, in local winter (Figures 2b, 2c, 2f, 2g), the nightime variation becomes more pronounced than in the daytime; moreover, the cone angle dependence between the daytime and nighttime is different. For example, in the summer NH (Figure 2e), the daytime westward PEJ shows its maximum value around 60°–90° (i.e. IMF $B_x > 0$). In the winter NH (Figures 2c, 2g), the

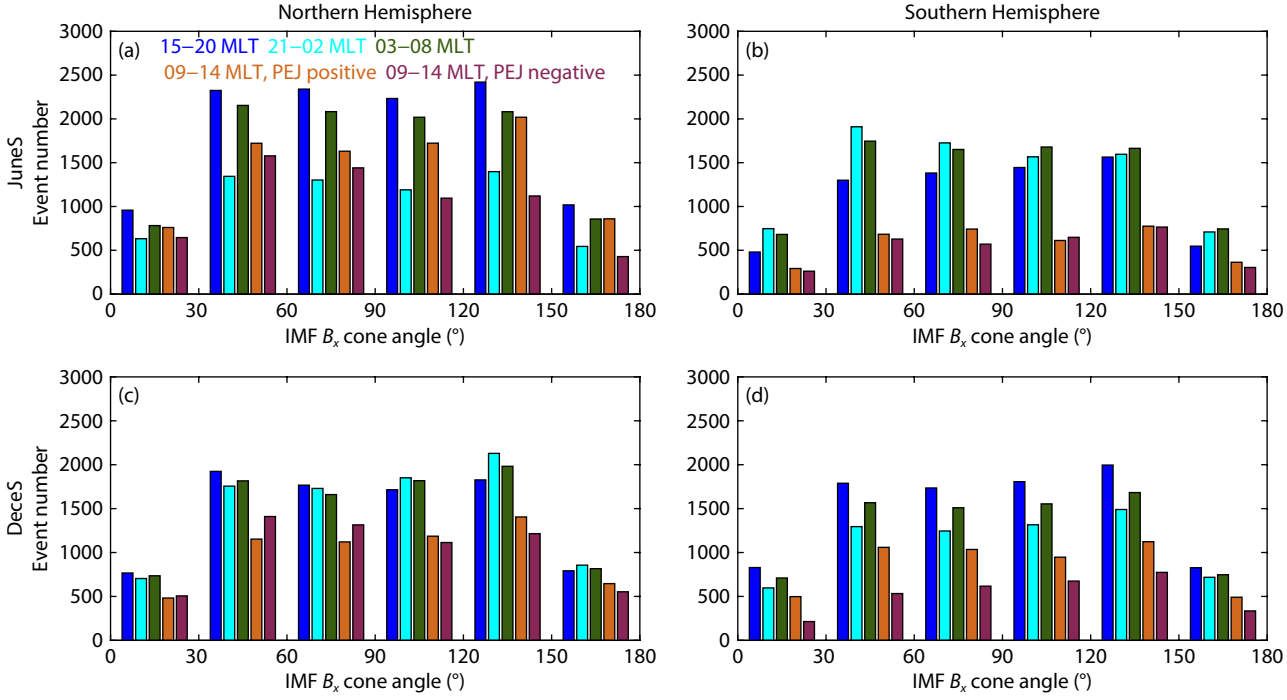

Figure 1. Counts of auroral crossings events, recorded by CHAMP and Swarm A, as a function of IMF B_x cone angle when E_m is less than 3 mV/m. The data are divided into two panels: the left panel presents Northern Hemisphere event counts; the right panel presents Southern Hemisphere counts. The bars are color-coded to distinguish among different local time sectors.

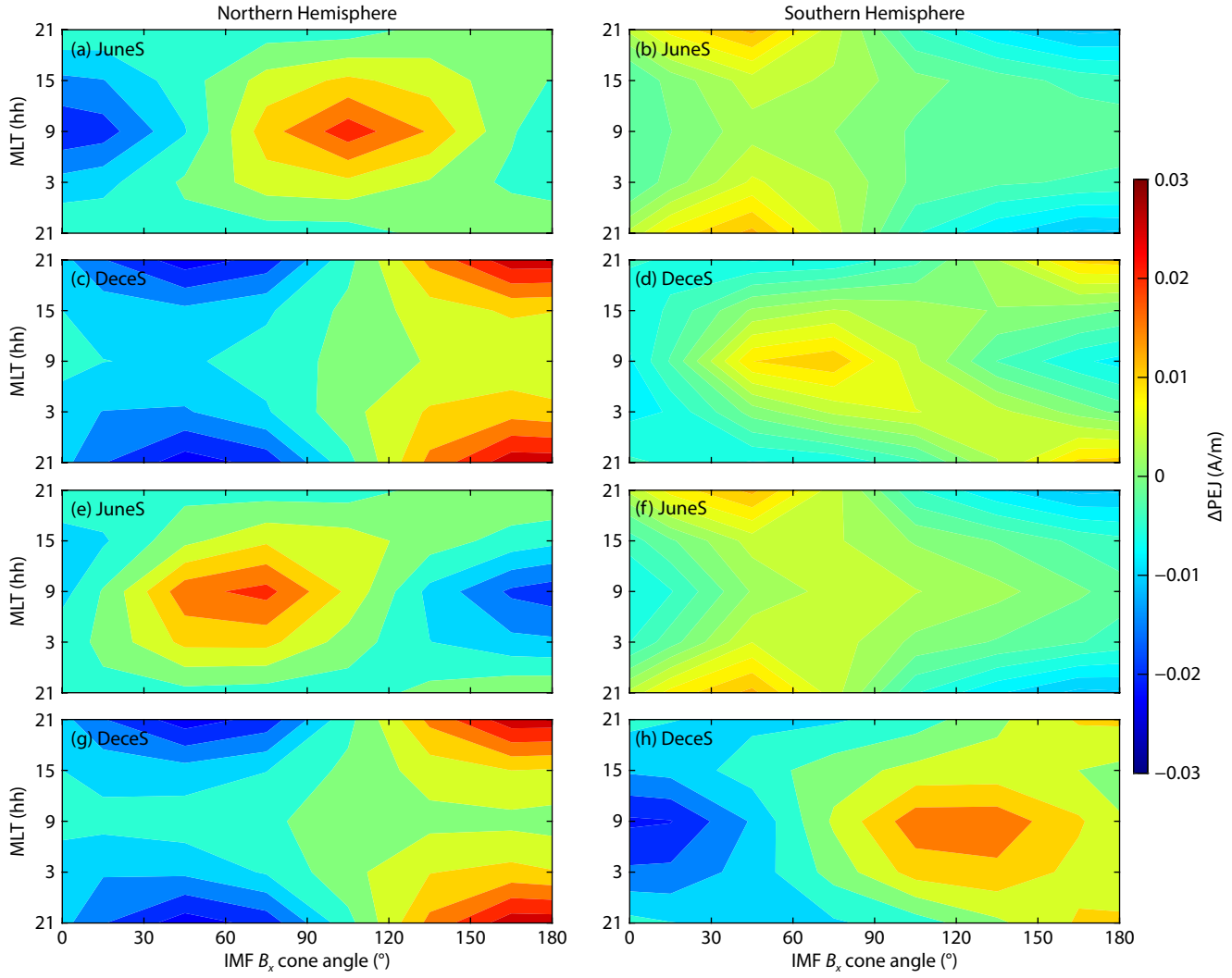

Figure 2. IMF B_x cone angle versus magnetic local time variations of absolute PEJ in the Northern (left column) and Southern (right column) Hemispheres. Panels (a)–(d) are for positive PEJ around noon; (e)–(h) are for for negative PEJ around noon. The mean value has been subtracted in each local time. Panels (a), (b), (e), and (f) are June solstice; (c), (d), (g), and (h) are December solstice.

nighttime westward PEJ shows its maximum value around 120°–180° (i.e. IMF B_x < 0). The B_x sign dependence of eastward and westward PEJ around noontime is nearly opposite. The noontime eastward PEJ (Figure 2a) in the NH shows its maximum value at IMF B_x < 0, while the noontime westward PEJ (Figure 2e) shows its maximum value at IMF B_x > 0. The variation of PEJ with IMF B_x is less prominent at dawn and dusk when compared to the noon and midnight sectors. The response of noontime and midnight PEJ to the IMF B_x sign in the Southern Hemisphere is reversed when compared to that in the Northern Hemisphere.

One can notice that the peak value of PEJ around noon (Figures 2a, 2d, 2e, 2f, 2h) aligns around cone angle 90°, while the minimum value aligns near 0° or 180°, indicating that the influences of IMF B_y and B_z surpass that of the IMF B_x component. However, during nighttime (Figures 2b, 2c, 2d, 2f, 2g, 2h), the maximum PEJ shift towards 0° or 180°, indicating that the effect of IMF B_x on the nighttime PEJ might surpass that of IMF B_y or B_z.

Figure 3 shows the difference in the MLat ($\Delta MLat$) of peak PEJ as a function of IMF B_x cone angle and local time in the same format as Figure 2. The mean absolute MLat of PEJ within each local time under all IMF B_x cone angle conditions is determined and is then subtracted in each local time in order to better represent peak PEJ variation in latitude with IMF B_x cone angle. One can notice that the most prominent response occurs around noon and midnight, with the dawn and dusk less affected. Changes in the summer hemisphere are notably greater compared to those in the winter hemisphere. PEJ locations show local time and hemispheric asymmetry in their dependence on the IMF B_x orientation. During the Northern Hemisphere's summer, the noontime eastward PEJ (Figure 3a) is positioned at a higher latitude when IMF B_x < 0 (cone angle >90°), while the noontime westward PEJ (Figure 3e) and nighttime westward PEJ (Figures 3a, 3c, 3e, 3g) are situated at higher latitudes when IMF B_x > 0 (cone angle <90°). In contrast, during the Southern Hemisphere's summer, the eastward PEJ at noon (Figure 3d) is located at a higher latitude when IMF B_x > 0, whereas the westward PEJ at noon (Figure 3h) and night (Figures 3b, 3d, 3f, 3h) is positioned at a higher latitude when IMF B_x < 0.

In order to separate the impact of IMF B_x from the other IMF

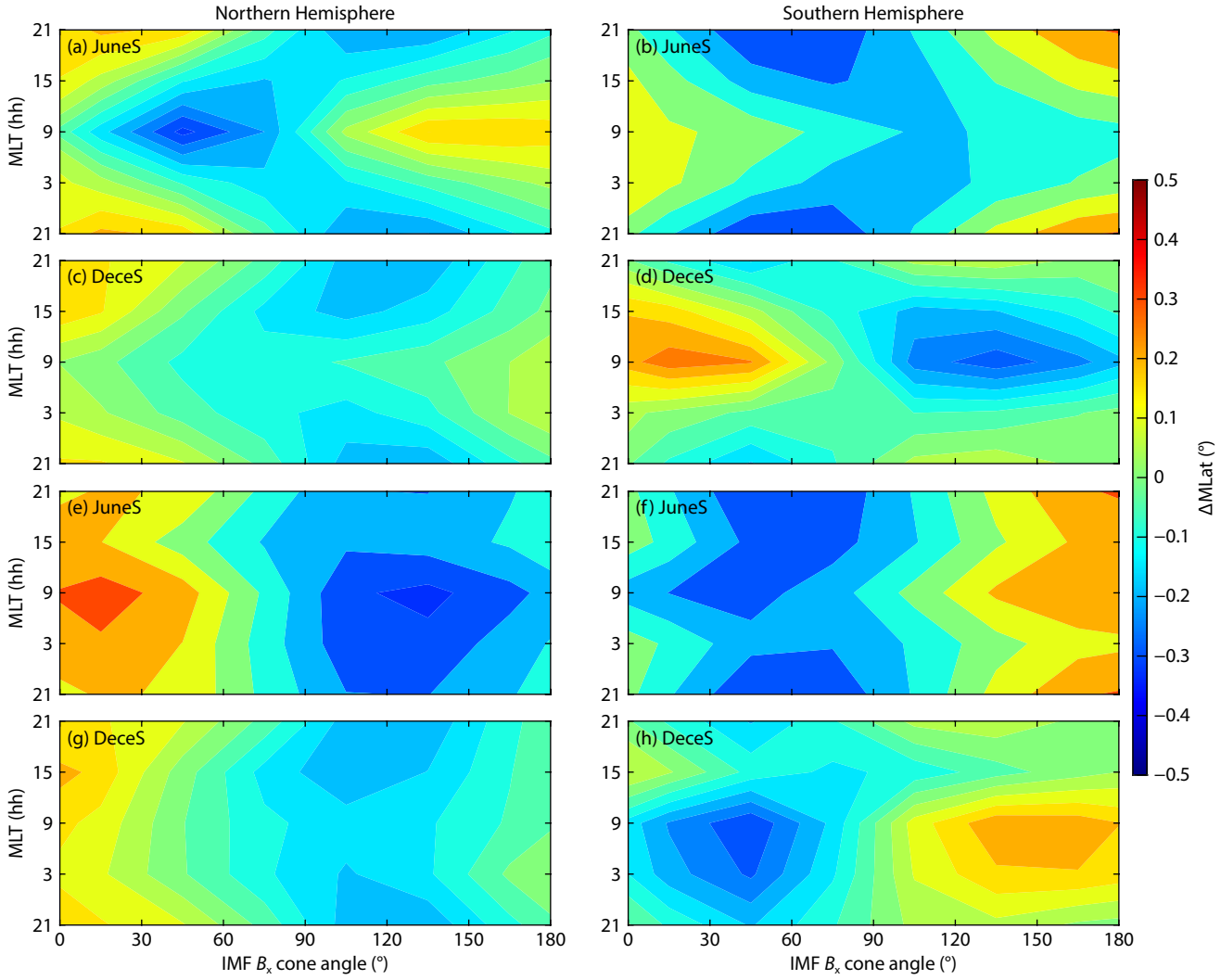

Figure 3. The same format as Figure 2, but for the MLat of peak PEJ. IMF B_x cone angle versus magnetic local time variations of the MLat of peak PEJ in the Northern (left column) and Southern Hemispheres (right column). Panels (a)–(d) are for positive PEJ around noon, and (e)–(h) for negative PEJ around noon. The mean value has been subtracted in each local time. Panels (a), (b), (e), and (f) are in June solstice and (c), (d), (g), and (h) are in December solstice.

components, we have subtracted the result of dominant IMF $B_x > 0$ (i.e. cone angle ≤30°) from that of IMF $B_x < 0$ (i.e. cone angle ≥150°) to obtain ΔPEJ and $\Delta MLat$, i.e.

$$\Delta PEJ = |\text{PEJ}| \text{ cone angle} \leq 30° - |\text{PEJ}| \text{ cone angle} \geq 150°,$$

and

$$\Delta MLat = |\text{MLat}| \text{ cone angle} \leq 30° - |\text{MLat}| \text{ cone angle} \geq 150°.$$

The closer the cone angle is to 0° or 180°, the more influential the B_x component becomes. Such explicit impact of the orientation of IMF B_x on the strength and position of PEJ is illustrated in Figure 4. A positive value means the current is stronger and its location is at a higher latitude for IMF $B_x > 0$ than for IMF $B_x < 0$. The asterisk denotes the summer solstice; the circle denotes the winter solstice. The blue dashed line indicates the Northern Hemisphere; the red dashed line indicates the Southern Hemisphere.

For the eastward PEJ in the dusk sector (15–20 MLT), in both hemispheres, the ΔPEJ of IMF $B_x > 0$ is a little weaker than that of IMF $B_x < 0$, a difference more evident in NH summer. For IMF $B_x > 0$, the latitude of the PEJ is located a little more poleward than that of IMF $B_x < 0$, except for that in the winter SH. In the 21–02 MLT sector, the westward current is obviously weaker for IMF $B_x > 0$ than for IMF $B_x < 0$ in local NH winter, while the PEJ is obviously stronger for IMF $B_x > 0$ than for IMF $B_x < 0$ during the local SH winter. A weaker IMF B_x effect can be observed in the local summer hemisphere. The NH PEJ for IMF $B_x > 0$ is located at a higher latitude than for IMF $B_x < 0$, while the SH PEJ shows an opposite trend. The IMF B_x dependence of the westward electrojet in the dawn sector (03–08 MLT) is less obvious than in the nighttime (21–02 MLT). In the summer NH, the PEJ is stronger for IMF $B_x > 0$, while in the winter NH, the PEJ of IMF $B_x < 0$ is stronger. The SH response is weaker than that in the NH. The PEJ for IMF $B_x > 0$ is located at higher latitudes, compared to that for IMF $B_x < 0$, except for the SH summer. Around noontime, the responses of the eastward and westward PEJ to IMF B_x are more significant in local summer. For IMF $B_x > 0$ (IMF $B_x < 0$), the eastward (westward) PEJ in the NH is weaker and located at lower latitudes, whereas the

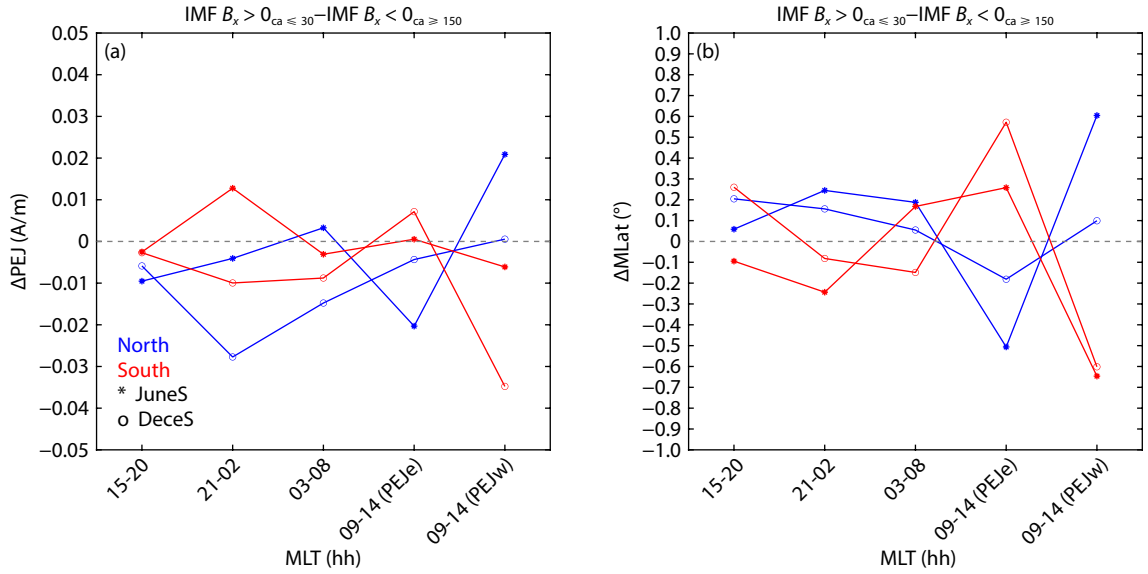

Figure 4. Variations of absolute peak PEJ and MLat between IMF cone angle ≤30° and cone angle ≥150° as a function of MLT. The asterisk denotes June solstice, and the circle represents December solstice. Blue lines indicate Northern Hemisphere data; red lines, Southern Hemisphere.

opposite effect is true in the SH, with the latitudinal differences being greater in local summer than in local winter. This confirms the effect of ionospheric conductance on the MLat of PEJ, i.e., the auroral region retreats equatorward under dark conditions (Wang H et al., 2005).

We further calculate the relative change of PEJ compared to the background value, which is defined as $\Delta PEJ/M_{PEJ}$. The average peak PEJ values for IMF B_x cone angles ≤30° and ≥150° is defined as

$$M_{PEJ} = 0.5 \times (|\text{PEJ}|\text{cone angle} \leq 30° + |\text{PEJ}|\text{cone angle} \geq 150°).$$

Notably, the changes in PEJ density during winter night and summer day can reach nearly 6%–22% relative to background values, differences that can be regarded significant.

4. Discussion

In this study, we investigate differences in local time and hemispheric impact of IMF B_x on peak PEJ current density and MLat by examining more than 16 years of observations from CHAMP (2000–2010) and Swarm (2014–2020) satellites. We find that IMF B_x has obvious impacts on the latitude and peak strength of PEJs; prominent local time, seasonal, and hemispheric differences in both are well correlated with variations in IMF B_x.

This study examines periods dominated by IMF B_x. When the IMF cone angle is ≤30° or ≥150°, IMF is primarily aligned sunward or anti-sunward, and the IMF B_y and B_z are relatively weaker compared to IMF B_x. As E_m is primarily associated with the amplitudes of IMF B_y and B_z, it remains weak during times when IMF B_x prevails.

Figure 5 illustrates the variation of IMF B_x, B_y, B_z, and E_m between periods of IMF cone angle ≤30° (IMF $B_x > 0$) and IMF cone angle ≥150° (IMF $B_x < 0$) in different local time sectors. It reveals a difference of about −1.2 nT in IMF B_y, about 0.25 nT in IMF B_z, about 0.05 mV/m in E_m. However, these fluctuations appear insufficient to explain the 6–20% variations observed in PEJ strength during midnight and noon periods. Previous researchers have studied the impact of IMF B_x on the *AL* index, and have typically restricted IMF $|B_y|$ to less than 1 nT (Laundal et al., 2018b) or less than 2 nT (Holappa et al., 2023) in order to eliminate the influence of IMF B_y. In our study, the variation in IMF B_y falls within these specified ranges. However, IMF B_x variance exceeds 4 nT, suggesting that the differences in local time, season, and hemisphere in PEJ strength and latitude, as revealed in Figure 4, stem primarily from the influence of IMF B_x.

Overall, the explicit effect of IMF B_x is more pronounced around noontime and midnight, compared to dawn and dusk sectors. This might be attributed to the alignment of IMF B_x along the noon-meridional direction. Notably, the IMF B_x effect on the westward PEJ near midnight (21–02 MLT) is more significant in winter than in summer. During NH winter, when IMF $B_x < 0$, the westward PEJ is stronger than when IMF $B_x > 0$; conversely, in SH winter, the westward electrojet is stronger for IMF $B_x > 0$ compared to IMF $B_x < 0$. This result is consistent with previous studies (Kubyshkina et al., 2023), indicating that in NH winter, IMF $B_x > 0$ suppresses the *AL* index while $B_x < 0$ increases *AL* under similar driving conditions. Kubyshkina et al. (2023) explained that IMF B_x could impact the nightside magnetospheric configuration, causing a shift in the current sheet either northward or southward for IMF $B_x < 0$ or $B_x > 0$. In cases of a large negative dipole tilt (i.e. NH winter) with plasma sheet positioned below the equatorial plane, IMF $B_x < 0$ might realign the current sheet back towards the equatorial plane, restoring symmetry and resulting in increased aurora activity. A similar scenario arises in SH winter with a large positive dipole tilt for IMF $B_x > 0$.

Another explanation for the winter preference of IMF B_x effect on the nighttime PEJ is related to the nighttime aurora precipitation. In local winter, ionospheric conductance is induced mainly by particle precipitation, whereas in local summer, solar illuminated ionospheric conductance dominates. Particle precipitation shows

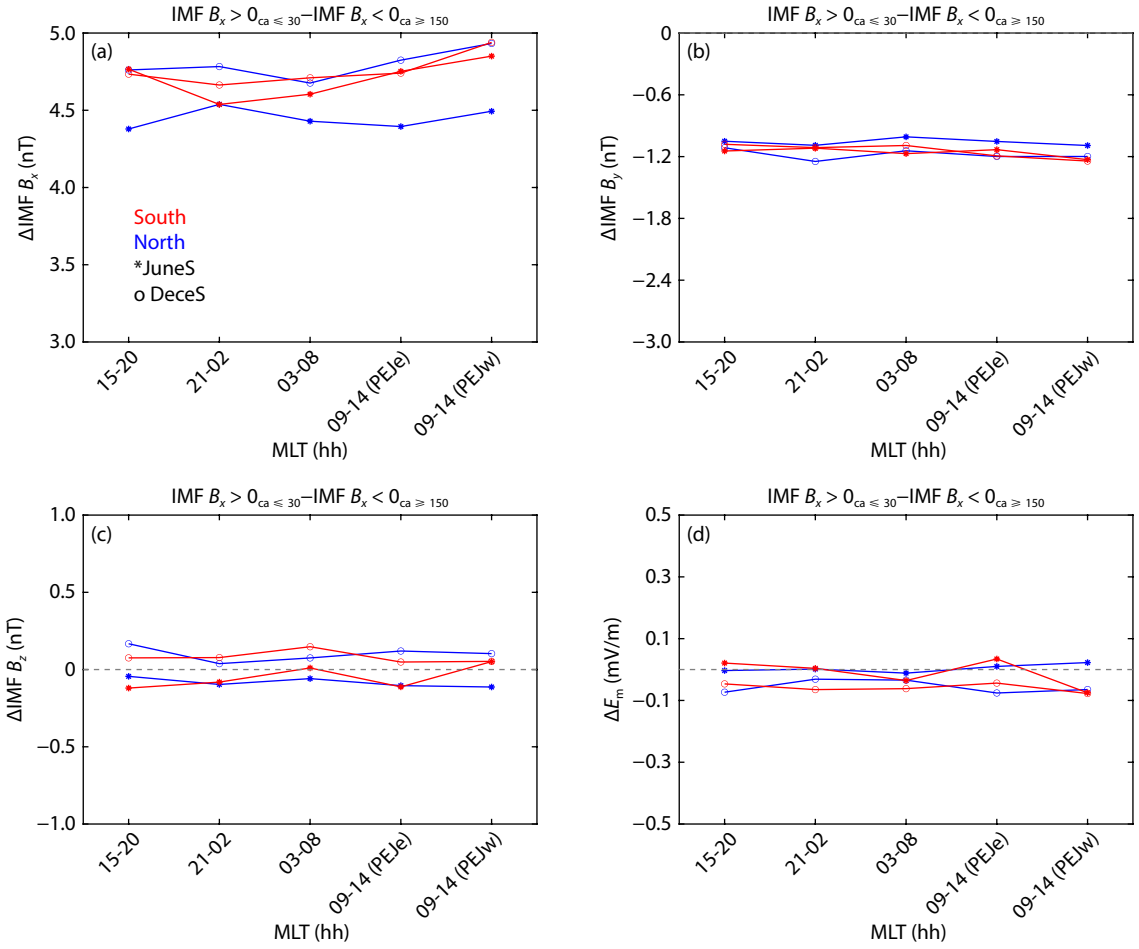

Figure 5. Differences of IMF B_x, B_y, B_z, and E_m between IMF cone angle ≤30° and cone angle ≥150° as a function of MLT. The asterisk denotes June solstice, and the circle represents December solstice. Blue lines represent Northern Hemisphere data; red lines, Hemisphere.

explicit IMF B_x dependence. Shue et al. (2002) reported that the NH nighttime auroral power was higher for IMF $B_x < 0$ than for IMF $B_x > 0$ under similar IMF B_y conditions when IMF is southward. The opposite trend was observed in the SH. This IMF B_x dependence of auroral intensity was further confirmed by Reistad et al. (2014). This might explain why the IMF B_x effect on PEJs is relatively more pronounced in local winter compared to local summer.

Unlike the midnight sector, the IMF B_x effect on the noontime PEJ is more significant in the summer hemisphere with higher conductance. During periods dominated by IMF $B_x < 0$ ($B_x > 0$), the reconnection site tends to manifest around the northern (southern) magnetotail lobe, facilitating antiparallel reconnection between the earthward (sunward) IMF B_x and the northward geomagnetic field. In summer, the magnetotail shifts closer to the Sun, creating a geomagnetic geometry more conducive to lobe reconnection. Lobe reconnection seems to explain why the noontime PEJ in the NH is situated at a higher latitude when IMF $B_x < 0$, as compared to when IMF $B_x > 0$. Conversely, in the SH, the reversed IMF B_x sign effect occurs: IMF $B_x > 0$ promotes the southern lobe reconnection, resulting in a larger PEJ located at a higher latitude in the SH.

In the Northern Hemisphere, the eastward current is stronger when IMF $B_x < 0$ than when IMF $B_x > 0$, while the westward PEJ shows a reversed variation with the IMF B_x sign. Conversely, the SH PEJ shows the opposite IMF B_x sign dependence. One plausible explanation might be that in the NH, IMF $B_x < 0$ results in a larger eastward PEJ, whereas in the SH, it is IMF $B_x > 0$ that results in enhanced eastward PEJ. This also explains why the westward PEJ gets weakened in the NH during IMF $B_x < 0$ compared to IMF $B_x > 0$, as the negative B_x strengthens the eastward PEJ. Therefore, the pre-existing westward PEJ gets reduced and the center of peak westward PEJ shifts toward lower latitudes.

When IMF $B_x < 0$, the eastward current intensifies on the dayside of NH, which might be attributed to the magnetic tension force acting on open field lines during IMF B_x periods. As proposed by Cowley (1981) and Reistad et al. (2014), negative (positive) IMF B_x results in a larger magnetic tension force on the northern (southern) open magnetic field line. This amplifies the magnetopause current perpendicular to the magnetic field, flowing into the noon-midnight meridional plane when observed from the duskside. This magnetopause current, known as the generator of FACs, strengthens and flows into the ionosphere in the pre-noon sector but flows out of the ionosphere in the post-noon sector. Consequently, an enhanced ionospheric eastward current is expected to connect FACs around noontime. Although the direction of PEJs has been regarded to be controlled by IMF B_y (e.g., Friis-Christensen and Wilhjelm, 1975), this work suggests that the direction of the

IMF B_x component, too, impacts the flow direction of the noontime PEJ, with a more significant impact in the summer hemisphere.

5. Summary

In the present work, we have studied the important impact of IMF B_x on PEJ peak current density and location. Our study is based on magnetic field observations gathered from CHAMP (2000–2010) and Swarm (2014–2020) satellites. The effect of IMF B_x on PEJ strength and location displays obvious local time, seasonal, and hemispherical differences, suggesting distinct dominant physical processes in different local time sectors.

Generally, IMF tend to amplify the westward PEJ in the *midnight* sectors when IMF $B_x < 0$ in the Northern Hemisphere (NH), and when IMF $B_x > 0$ in the Southern Hemisphere (SH). This effect is relatively stronger in the local winter hemisphere. Meanwhile, in the *noon* regions, IMF B_x intensifies the eastward current, consequently reducing the westward current, when it is <0 in the NH and when it is >0 in the SH; this pattern is stronger in the local summer. At *dusk and dawn*, the effect of IMF B_x on the PEJs is significantly weaker than in other local time sectors.

In addition, latitudinal positions of the NH and SH PEJs are unconjugated, but each does correlate with the orientations of its IMF B_x. For both the eastward and westward PEJs around noon and midnight, the dependence on IMF B_x polarity of hemispheric latitude displacement of PEJ is entirely opposite. When IMF $B_x < 0$ (IMF $B_x > 0$) in the NH (SH), the eastward current around noon shifts towards higher latitudes, while the westward current around midnight moves towards lower latitudes.

Acknowledgments

The authors greatly appreciate the web availability of data. The authors are grateful for support from the National Key Research and Development Program (2022YFF0503700), National Natural Science Foundation of China (42374200), and the National Natural Science Foundation of China Basic Science Center (42188101).

We gratefully acknowledge the CHAMP team for processing and providing the CHAMP scalar magnetic field data that are at http://doi.org/10.5880/GFZ.2.3.2019.004. The Swarm line model PEJ data are from the website https://swarm-diss.eo.esa.int/#swarm%2FLevel2daily%2FLatest_baselines%2FAEJ%2FLPL. The solar wind and interplanetary magnetic field and magnetic activity index data are from NASA/GSFC'S Space Physics Data Facility's OMNIWeb (https://omniweb.gsfc.nasa.gov).

References

Aakjær, C. D., Olsen, N., and Finlay, C. C. (2016). Determining polar ionospheric electrojet currents from *Swarm* satellite constellation magnetic data. *Earth, Planet Space, 68*(1), 140. https://doi.org/10.1186/S40623-016-0509-Y

Cowley, S. W. H. (1981). Asymmetry effects associated with the X-component of the IMF in a magnetically open magnetosphere. *Planet. Space Sci.*, *29*(8), 809–818. https://doi.org/10.1016/0032-0633(81)90071-4

Elphinstone, R. D., Jankowska, K., Murphree, J. S., and Cogger, L. L. (1990). The configuration of the auroral distribution for interplanetary magnetic field B_z northward: 1. IMF B_x and B_y dependencies as observed by the Viking satellite. *J. Geophys. Res.: Space Phys.*, *95*(A5), 5791–5804. https://doi.org/10.1029/JA095iA05p05791

Emmert, J. T., Richmond, A. D., and Drob, D. P. (2010). A computationally compact representation of Magnetic-Apex and Quasi-Dipole coordinates with smooth base vectors. *J. Geophys. Res.: Space Phys.*, *115*(A8), A08322. https://doi.org/10.1029/2010JA015326

Friis-Christensen, E., and Wilhjelm, J. (1975). Polar cap currents for different directions of the interplanetary magnetic field in the *Y-Z* plane. *J. Geophys. Res.*, *80*(10), 1248–1260. https://doi.org/10.1029/JA080i010p01248

Gjerloev, J. W., and Hoffman, R. A. (2014). The large-scale current system during auroral substorms. *J. Geophys. Res.: Space Phys.*, *119*(6), 4591–4606. https://doi.org/10.1002/2013JA019176

Guo, J. P., Liu, H. X., Feng, X. S., Pulkkinen, T. I., Tanskanen, E. I., Liu, C. X., Zhong, D. K., and Wang, Y. (2014). MLT and seasonal dependence of auroral electrojets: IMAGE magnetometer network observations. *J. Geophys. Res.: Space Phys.*, *119*(4), 3179–3188. https://doi.org/10.1002/2014JA019843

Hoilijoki, S., Souza, V. M., Walsh, B. M., Janhunen, P., and Palmroth, M. (2014). Magnetopause reconnection and energy conversion as influenced by the dipole tilt and the IMF B_x. *J. Geophys. Res.: Space Phys.*, *119*(6), 4484–4494. https://doi.org/10.1002/2013JA019693

Holappa, L., Reistad, J. P., and Ohma, A. (2023). Comment on "unraveling the role of IMF B_x in driving geomagnetic activity" by Kubyshkina et al. *J. Geophys. Res.: Space Phys.*, *128*(10), e2023JA031701. https://doi.org/10.1029/2023JA031701

Huang, T., Wang, H., Shue, J. H., Cai, L., and Pi, G. (2015). The dayside magnetopause location during radial interplanetary magnetic field periods: Cluster observation and model comparison. *Ann Geophys.*, *33*(4), 437–448. https://doi.org/10.5194/angeo-33-437-2015

Huang, T., Lühr, H., and Wang, H. (2017). Global characteristics of auroral Hall currents derived from the Swarm constellation: Dependences on season and IMF orientation. *Ann. Geophys.*, *35*(6), 1249–1268. https://doi.org/10.5194/angeo-35-1249-2017

Kivelson, M. G., and Hughes, W. J. (1990). On the threshold for triggering substorms. *Planet. Space Sci.*, *38*(2), 211–220. https://doi.org/10.1016/0032-0633(90)90085-5

Kubyshkina, M., Semenov, V., Erkaev, N., Gordeev, E., Dubyagin, S., Ganushkina, N., and Shukhtina, M. (2018). Relations between v_z and B_x components in solar wind and their effect on substorm onset. *Geophys. Res. Lett.*, *45*(9), 3760–3767. https://doi.org/10.1002/2017GL076268

Kubyshkina, M. V., Semenov, V. S., Tsyganenko, N. A., Wang, X. G., and Kubyshkin, I. V. (2023). Unraveling the role of IMF B_x in driving geomagnetic activity. *J. Geophys. Res.: Space Phys.*, *128*(4), e2022JA031275. https://doi.org/10.1029/2022JA031275

Laundal, K. M., Finlay, C. C., Olsen, N., and Reistad, J. P. (2018a). Solar wind and seasonal influence on ionospheric currents from swarm and CHAMP measurements. *J. Geophys. Res.: Space Phys.*, *123*(5), 4402–4429. https://doi.org/10.1029/2018JA025387

Laundal, K. M., Reistad, J. P., Finlay, C. C., Østgaard, N., Tenfjord, P., Snekvik, K., and Ohma, A. (2018b). Interplanetary Magnetic Field B_x component influence on horizontal and field-aligned currents in the ionosphere. *J. Geophys. Res.: Space Phys.*, *123*(5), 3360–3379. https://doi.org/10.1002/2017JA024864

Olsen, N. (1996). A new tool for determining ionospheric currents from magnetic satellite data. *Geophys. Res. Lett.*, *23*(24), 3635–3638. https://doi.org/10.1029/96GL02896

Reigber, C., Lühr, H., and Schwintzer, P. (2002). CHAMP mission status. *Adv. Space Res.*, *30*(2), 129–134. https://doi.org/10.1016/s0273-1177(02)00276-4

Reistad, J. P., Østgaard, N., Laundal, K. M., Haaland, S., Tenfjord, P., Snekvik, K., Oksavik, K., and Milan, S. E. (2014). Intensity asymmetries in the dusk sector of the poleward auroral oval due to IMF B_x. *J. Geophys. Res.: Space Phys.*, *119*(12), 9497–9507. https://doi.org/10.1002/2014JA020216

Reistad, J. P., Laundal, K. M., Ohma, A., Moretto, T., and Milan, S. E. (2020). An explicit IMF B_y dependence on solar wind-magnetosphere coupling. *Geophys. Res. Lett.*, *47*(1), e2019GL086062. https://doi.org/10.1029/2019GL086062

Richmond, A. D. (1995). Ionospheric electrodynamics using magnetic apex coordinates. *J. Geomagn. Geoelectr.*, *47*(2), 191–212. https://doi.org/10.5636/jgg.47.191

Ritter, P., Lühr, H., Maus, S., and Viljanen, A. (2004). High-latitude ionospheric

currents during very quiet times: Their characteristics and predictability. *Ann. Geophys.*, *22*(6), 2001–2014. https://doi.org/10.5194/angeo-22-2001-2004

Shue, J. H., Newell, P. T., Liou, K., and Meng, C. I. (2002). Solar wind density and velocity control of auroral brightness under normal interplanetary magnetic field conditions. *J. Geophys. Res.: Space Phys.*, *107*(A12), 1428. https://doi.org/10.1029/2001JA009138

Wang, H., Lühr, H., and Ma, S. Y. (2005). Solar zenith angle and merging electric field control of field-aligned currents: A statistical study of the Southern Hemisphere. *J. Geophys. Res.: Space Phys.*, *110*(A3), A03306. https://doi.org/10.1029/2004JA010530

Wang, H., Lühr, H., Ridley, A., Ritter, P., and Yu, Y. (2008). Storm time dynamics of auroral electrojets: CHAMP observation and the Space Weather Modeling Framework comparison. *Ann. Geophys.*, *26*(3), 555–570. https://doi.org/10.5194/angeo-26-555-2008

Wang, H., Lühr, H., Shue, J. H., Frey, H. U., Kervalishvili, G., Huang, T., Cao, X., Pi, G., and Ridley, A. J. (2014). Strong ionospheric field-aligned currents for radial interplanetary magnetic fields. *J. Geophys. Res.: Space Phys.*, *119*(5), 3979–3995. https://doi.org/10.1002/2014JA019951

Wang, H., and Lühr, H. (2023). Magnetic longitudinal and local time variations of polar electrojet and field-aligned currents. *J. Geophys. Res.: Space Phys.*, *128*(10), e2023JA031874. https://doi.org/10.1029/2023JA031874

Wang, H., and Lühr, H. (2024). IMF B_y effects on the strength and latitude of polar electrojets: CHAMP and swarm joint observations. *J. Geophys. Res.: Space Phys.*, *129*(1), e2023JA032049. https://doi.org/10.1029/2023JA032049

Wang, Y. B., Zhang, Y., Wang, Y. J., Liu, P. F., Cheng, J. X., Li, X. Z., Tang, K., Li, L. G., and Duan, X. W. (2023). Influences of various space current systems on the geomagnetic field in near-Earth space. *Earth Planet. Phys.*, *7*(1), 93–99. https://doi.org/10.26464/epp2023010

Zhong, Y. F., Wang, H., Zhang, K. D., Xia, H., and Qian, C. Y. (2022). Local Time response of auroral electrojet during magnetically disturbed periods: DMSP and CHAMP coordinated observations. *J. Geophys. Res.: Space Phys.*, *127*(8), e2022JA030624. https://doi.org/10.1029/2022JA030624